Multifragmentation at the energy of vanishing flow in central heavy-ion collisions

Jatinder K. Dhawan and Rajeev K. Puri
Physics Department, Panjab University, Chandigarh 160 014, India
(Received 31 May 2006; published 27 November 2006)

We studied the fragmentation of colliding nuclei at the energy of vanishing flow and evaluated its mass dependence throughout the periodic table. This study was performed within the framework of the quantum molecular dynamics model, which has been reported to reproduce the experimental data at low incident energies quite nicely. We simulated as many as 11 reactions for which the balance energy had been measured experimentally. Our observations at the energy of vanishing flow clearly suggest the existence of a power law system mass dependence for various fragment multiplicities. The power factor $\tau(\propto A^{\tau})$ is close to $(-1/3)$, as has also been reported for the mass dependence of the energy of vanishing flow. Experiments are needed to verify these predictions.

DOI: 10.1103/PhysRevC.74.054610 PACS number(s): 25.70.Pq, 24.10.Lx

I. INTRODUCTION

The collective flow measured/predicted in a heavy-ion collision is one of the few quantities/observables that are sensitive to the reaction ingredients and have been investigated extensively over the last two decades [1–25]. The study of collective flow also gives insight into the reaction dynamics as well as into the hot and dense nuclear matter formed in a reaction. One also wants to shed light on the equation of state and on the nucleonic cross section—one of the ultimate goals of heavy-ion collisions [1–25]. The collective flow (and its nature) depends crucially on several factors such as the size of the system, colliding geometry (i.e., the impact parameter), and incident energy of the projectile.

The reaction dynamics at low incident energies is governed by the attractive mean field that prompts the emission of particles into the backward hemisphere. Whereas the dominance at higher incident energies is due to the binary nucleon-nucleon collisions causing the particle emission into the forward hemisphere. While going from the low to higher incident energies, the collective transverse flow, at a particular incident energy, passes through a zero balance point [1–23]. This energy point is called the energy of vanishing flow (EVF) or, alternatively, the balance energy [1–23]. The EVF has been assumed to be helpful in finding the equation of state and/or the nucleonic cross sections. A connection between balance energy and critical liquid-gas phase transition (with a power law fragment mass dependence) has also been put forward in the literature [24]. During the last few years, extensive efforts have been made to measure and understand the energy of vanishing flow [1–23].

Recently, one of us and collaborators [22–23] presented a dynamic calculation of the EVF ranging between ^{12}C+^{12}C and ^{238}U+^{238}U reactions. There, an $A^{-1/3}$ dependence was obtained, and some information about the nucleonic cross sections was extracted. The experimental studies measured the balance energy between mass 24 and mass 394 [1–23]. Recently, one study has also reported the balance energy of ^{197}Au+^{197}Au reactions [13]. This extraction is based on the minimum in the excitation function of the flow which has been interpreted as the balance between the attraction and repulsive components of the nuclear interactions.

It is worth mentioning that only a few attempts discuss other variables such as density, temperature, and nucleon-nucleon binary collisions apart from the participant-spectator matter at the energy of vanishing flow [10,15–18,21–23]. Unfortunately, no study exists in the literature so far that sheds light on the fragment's structure at the balance point. This is a very important area to study, as EVF represents the counterbalancing of the attractive and repulsive forces. This counterbalancing had led to the mass-independent participant-spectator matter at the balance point [23]. Since fragmentation depends on the role of attractive and repulsive forces, it is of interest to investigate the fragment structure at EVF.

One should also note that the energy range of the balance point over the periodic table is also very interesting (it varies between 207 MeV/nucleon for ^{12}C+^{12}C to 43 MeV/nucleon for ^{197}Au+^{197}Au) [22–23]. In this energy domain, one has fusion-fission, onset of multifragmentation, evaporation, and vaporization among others. For the lighter colliding systems, the reaction time is too short for global equilibrium to occur; whereas a longer reaction time in the heavier nuclei does allow the matter to equilibrate. As reported in Ref. [25], a significant portion of the colliding nucleons go into light as well as intermediate mass fragments. The light and intermediate mass fragments constitute about 2/3 and 1/3, respectively, at 150 MeV/nucleon, whereas they are 1/3 and 2/3 at 50 MeV/nucleon [25]. The complexity of the above mentioned phenomena [25] makes the present study further interesting. In view of the above cited reasons, it is highly desirous to study the fragment structure at the balance energy to see how mass dependence of the fragment structure behaves at EVF and whether power mass law (as obtained in the energy of vanishing flow) also exists for various fragments. Section II deals with the model, Sec. III is devoted to the results, and Sec. IV summarizes our findings.

II. THE MODEL

We describe the time evolution of a heavy-ion reaction within the framework of the quantum molecular dynamics (QMD) model [19–23,25–29] which is based on a molecular dynamics picture. Here, each nucleon is represented by a coherent state of the form

$$\phi_\alpha(x_1,t)=\left(\frac{2}{L\pi}\right)^{\frac{3}{4}} e^{-(x_1-x_\alpha(t))^2} e^{ip_\alpha(x_1-x_\alpha)} e^{-\frac{ip_\alpha^2 t}{2m}}. \quad (1)$$

Thus, the wave function has two time-dependent parameters x_α and p_α. The total n-body wave function is assumed to be a direct product of coherent states:

$$\phi=\phi_\alpha(x_1,x_\alpha,p_\alpha,t)\phi_\beta(x_2,x_\beta,p_\beta,t)\cdots, \quad (2)$$

where antisymmetrization is neglected. One should, however, keep in the mind that the other quantum features have been introduced. For instance, proper Fermi motion of nucleons is also implemented at the ground state. The initial values of the parameters are chosen in a way that the ensemble (A_T+A_P) nucleons give a proper density distribution as well as a proper momentum distribution of the projectile and target nuclei. The time evolution of the system is calculated using the generalized variational principle. We start out from the action

$$S=\int_{t_1}^{t_2}\mathcal{L}[\phi,\phi^*]d\tau, \quad (3)$$

with the Lagrange functional

$$\mathcal{L}=\left(\phi\left|i\hbar\frac{d}{dt}-H\right|\phi\right), \quad (4)$$

where the total time derivative includes the derivatives with respect to the parameters. The time evolution is obtained by the requirement that the action is stationary under the allowed variation of the wave function

$$\delta S=\delta\int_{t_1}^{t_2}\mathcal{L}[\phi,\phi^*]dt=0. \quad (5)$$

If the true solution of the Schrödinger equation is contained in the restricted set of wave functions $\phi_\alpha(x_1,x_\alpha,p_\alpha)$, this variation of the action gives the exact solution of the Schrödinger equation. If the parameter space is too restricted, we obtain that wave function in the restricted parameter space which comes close to the solution of the Schrödinger equation. Performing the variation with the test wave function (2), we obtain for each parameter λ a Euler-Lagrange equation

$$\frac{d}{dt}\frac{\partial\mathcal{L}}{\partial\dot{\lambda}}-\frac{\partial\mathcal{L}}{\partial\lambda}=0. \quad (6)$$

For each coherent state and a Hamiltonian of the form

$$H=\sum_\alpha\left[T_\alpha+\frac{1}{2}\sum_{\alpha\beta}V_{\alpha\beta}\right],$$

the Lagrangian and the Euler-Lagrange function can be easily calculated [26] as

$$\mathcal{L}=\sum_\alpha\dot{\mathbf{x}}_\alpha\mathbf{p}_\alpha-\sum_\beta\langle V_{\alpha\beta}\rangle-\frac{3}{2Lm}, \quad (7)$$

$$\dot{\mathbf{x}}_\alpha=\frac{\mathbf{p}_\alpha}{m}+\nabla_{p_\alpha}\sum_\beta\langle V_{\alpha\beta}\rangle, \quad (8)$$

$$\dot{\mathbf{p}}_\alpha=-\nabla_{\mathbf{x}_\alpha}\sum_\beta\langle V_{\alpha\beta}\rangle. \quad (9)$$

Thus, the variational approach has reduced the n-body Schrödinger equation to a set of $6n$ different equations for the parameters which can be solved numerically. If one inspects the formalism carefully, one finds that the interaction potential which is actually the Bruckner G-matrix can be divided into two parts: (i) a real part and (ii) an imaginary part. The real part of the potential acts like a potential, whereas the imaginary part is proportional to the cross section.

In the present model, the interaction potential comprises the following terms:

$$V_{\alpha\beta}=V_{\rm loc}^2+V_{\rm loc}^3+V_{\rm Coul}+V_{\rm Yuk}, \quad (10)$$

$V_{\rm loc}$ is the Skyrme force whereas $V_{\rm Coul}$ and $V_{\rm Yuk}$ define, respectively, the Coulomb and Yukawa terms. The expectation value of these potentials is calculated as

$$V_{\rm loc}^2=\int f_\alpha(\mathbf{p}_\alpha,\mathbf{r}_\alpha,t)f_\beta(\mathbf{p}_\beta,\mathbf{r}_\beta,t)V_I^{(2)}(\mathbf{r}_\alpha,\mathbf{r}_\beta)\times d^3\mathbf{r}_\alpha d^3\mathbf{r}_\beta d^3\mathbf{p}_\alpha d^3\mathbf{p}_\beta, \quad (11)$$

$$V_{\rm loc}^3=\int f_\alpha(\mathbf{p}_\alpha,\mathbf{r}_\alpha,t)f_\beta(\mathbf{p}_\beta,\mathbf{r}_\beta,t)f_\gamma(\mathbf{p}_\gamma,\mathbf{r}_\gamma,t)\times V_I^{(3)}(\mathbf{r}_\alpha,\mathbf{r}_\beta,\mathbf{r}_\gamma)\,d^3\mathbf{r}_\alpha d^3\mathbf{r}_\beta d^3\mathbf{r}_\gamma\times d^3\mathbf{p}_\alpha d^3\mathbf{p}_\beta d^3\mathbf{p}_\gamma. \quad (12)$$

Where $f_\alpha(\mathbf{p}_\alpha,\mathbf{r}_\alpha,t)$ is the Wigner density which corresponds to the wave functions (Eq. 2). If we deal with only the local Skyrme force, we get

$$V^{\rm Skyrme}=\sum_{\alpha=1}^{A_T+A_P}\left[\frac{A}{2}\sum_{\beta=1}\left(\frac{\tilde{\rho}_{\alpha\beta}}{\rho_0}\right)+\frac{B}{C+1}\sum_{\beta\neq\alpha}\left(\frac{\tilde{\rho}_{\alpha\beta}}{\rho_0}\right)^C\right]. \quad (13)$$

Here A, B, and C are the Skyrme parameters which are defined according to the ground state properties of a nucleus. Different values of C lead to different equations of state. A larger value of C (=380 MeV) is often dubbed as a stiff equation of state. The Pauli principle enters the calculations via the collision term only. A refined version in terms of constrained molecular dynamics has also been put forward recently [30].

III. RESULTS AND DISCUSSION

The literature contains a number of attempts to study the nature of the equation of state. Following Refs. [1,6,8,10, 17–23,31,32], we shall also employ a stiff equation of state throughout the present analysis. It should also be noted that the success rate is nearly the same for stiff and soft equations

of state. Furthermore, Refs. [6,10,17,18,32] have shown that the difference between $E_{\rm bal}$ using a stiff and that using a soft equation of state is insignificant for central heavy-ion collisions. Following Refs. [6,10,17,21–23,32–34], we also use a constant energy-independent cross section. As shown by Li [15], most of the collisions below 100 MeV/nucleon happen with nucleon-nucleon cross sections of 55 mb strength. Keeping the present energy domain in mind, the choice of a constant cross section is justified. It has also been shown by Zheng *et al.* [31] that a stiff equation of state with a free nucleon-nucleon cross section and a soft equation of state with a reduced cross section yield nearly the same results. The inclusion of momentum-dependent interactions has an influence in peripheral collisions, but their role is marginal in central collisions. Furthermore, the slope of the balance energy is also insensitive to the momentum dependence of the interaction [20]. We simulated each of the reactions of ^{36}Ar+^{27}Al ($b = 2$ fm), ^{40}Ar+^{27}Al ($b = 1.6$ fm), ^{40}Ar+^{45}Sc ($b/b_{\rm max} = 0.4$), ^{40}Ar+^{51}V ($b/b_{\rm max} = 0.3$), ^{64}Zn+^{48}Ti ($b = 2$ fm), ^{58}Ni+^{58}Ni($b/b_{\rm max} = 0.28$), ^{64}Zn+^{58}Ni ($b = 2$ fm), ^{86}Kr+^{93}Nb ($b/b_{\rm max} = 0.4$), ^{93}Nb+^{93}Nb ($b/b_{\rm max} = 0.3$), ^{139}La+^{139}La ($b/b_{\rm max} = 0.3$), and ^{197}Au+^{197}Au ($b = 2.5$ fm) for 1000–3000 events. As noted in Ref. [22], the impact parameter is guided by the experimental constraints. The incident energies, which are also the balance energies, read as 74, 67.3, 89.4, 67.8, 59.3, 62.6, 56.6, 69.2, 57, 51.6, and 43 MeV/nucleon, respectively, for the above reactions [22].

The QMD model had been robust against the findings of several experiments in the literature [25,35]. Interestingly, as noted in Ref. [25], the QMD model explains the fragments and charged-particle multiplicities in the symmetric reactions of Xe+Sn (at incident energies of 25, 32, and 50 MeV/nucleon) and Kr+Au (at incident energies between 55 and 200 MeV/nucleon) as well as in the highly asymmetric reactions of O+Br/Ag (at incident energies between 25 and 200 MeV/nucleon) [35]. One should note, however, that the agreement between the QMD model and experimental findings at the low energy tail is unexpected since the QMD model, being a semiclassical approach, lacks the refined quantum features needed at low incident energies. These examples clearly suggest that the QMD model explains the dynamics at the lower energy tail where a thermalized source is quite prominent. On the other hand, the same QMD model fails badly at higher incident energies ($E \geqslant 400$ MeV/nucleon) pointing toward a low momentum transfer from hot participant matter to spectator matter [36]. Since our present energy domain is at the lower tail of the incident energy (between 43 and 90 MeV/nucleon), the QMD model can be applied safely.

Every dynamic model follows the trajectory of individual nucleons only. Therefore, one has to clusterize the phase space at the end of the reaction to get the fragments. There are different secondary algorithms available in the literature that range from the simple spatial correlation method to complicated energy minimization algorithms [36]. In the present work, we shall use the simple spatial clusterization algorithm dubbed as the minimum spanning tree (MST) method where nucleons are bound in a fragment if the distance of two nucleons is smaller than 4 fm. As reported above, this algorithm works fine at mild excitation energies.

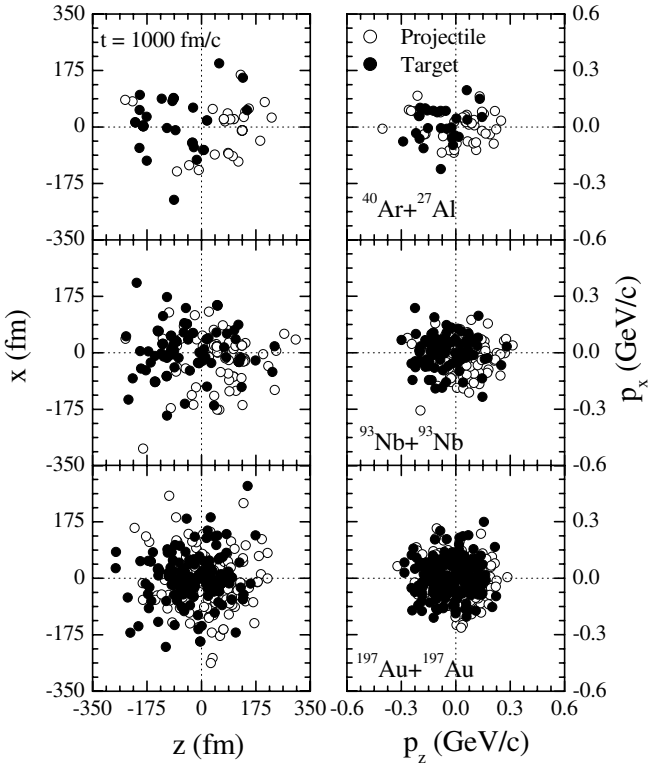

FIG. 1. Snapshots of a single event in the phase space (x, z), left side, and (p_x, p_z), right side, for the reactions ^{40}Ar+^{27}Al, ^{93}Nb+^{93}Nb, and ^{197}Au+^{197}Au at their corresponding balance energies of, respectively, 67.3, 57, and 43 MeV/nucleon.

In Fig. 1, we display the snapshots of the final phase space for a few reactions at the energy of vanishing flow. The saturation time, corresponding to the saturated flow, depends upon the reaction ingredients. We plot in Fig. 1, the (x, z) and (p_x, p_z) for the reactions of ^{40}Ar+^{27}Al, ^{93}Nb+^{93}Nb, and ^{197}Au+^{197}Au at 1000 fm/c. Interestingly, we see that the spatial space is quite similar and homogeneous in all three reactions. A single spherical distribution in the momentum space indicates a nearly thermalized source. The above picture is quite similar for a large number of different events indicating a uniform distribution. From the figure, one also notices that the blast mechanism is at its threshold. One may need even a higher incident energy for the participant-spectator demarcation. One may also conclude that a large part of the nucleons present in various fragments are preselected due to their initial phase space. The situation in these central collisions is pointing toward a semitransparent regime which will, of course, turn into a deep inelastic collision once we shift to peripheral collisions.

The phase space obtained during each time step is then clusterized using the MST method which yields the fragments of different sizes ranging from the free nucleons to deep spallation and fission residuals.

In Fig. 2, we display the time evolution of different fragments obtained in the above cited reactions at their corresponding theoretical balance energy. We display the largest fragment survived $A^{\rm max}$, emitted nucleons, light mass fragments (LMF's) $2 \leqslant A \leqslant 4$, medium mass frag-

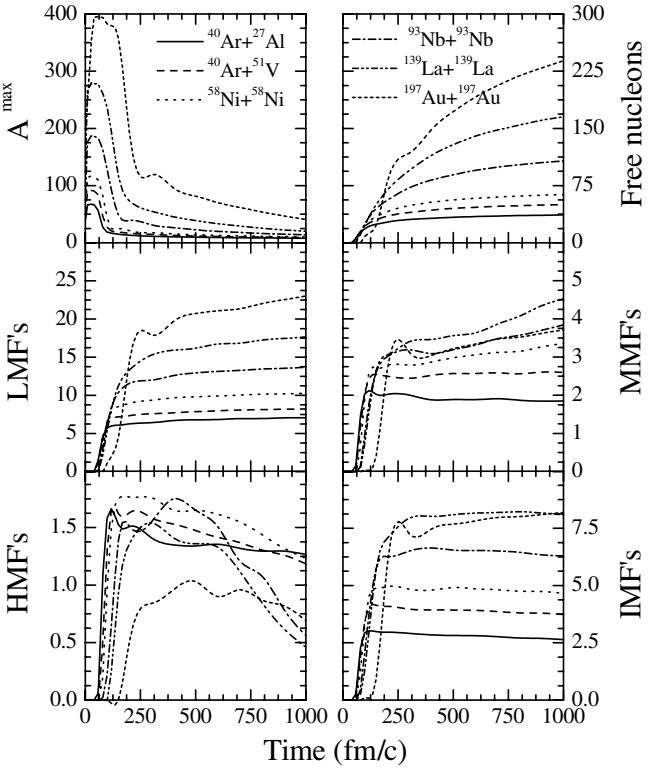

FIG. 2. Time evolution of the largest fragment $A^{\max}$, free nucleons, LMF's ($2 \leqslant A \leqslant 4$), MMF's ($5 \leqslant A \leqslant 11$), HMF's ($15\% \leqslant A \leqslant 30\%$), and IMF's ($4 \leqslant A \leqslant 30\%$) for the collisions of ^{40}Ar+^{27}Al, ^{40}Ar+^{51}V, ^{58}Ni+^{58}Ni, ^{93}Nb+^{93}Nb, ^{139}La+^{139}La, and ^{197}Au+^{197}Au at their corresponding theoretical balance energies of, respectively, 67.3, 67.8, 62.6, 57, 51.6, and 43 MeV/nucleon.

ments (MMF's) $5 \leqslant A \leqslant 11$, heavy mass fragments (HMF's) $15\% \leqslant A \leqslant 30\%$ as well as the intermediate mass fragments (IMF's) $4 \leqslant A \leqslant 30\%$ (of the largest between target and projectile). The percentages given in the HMF and IMF definitions are used to avoid unwanted and artificial heavy fragments that can appear in lighter colliding nuclei. As has been discussed by many authors [35], $A^{\max}$ has a peak around 50–100 fm/c. The excited compound nucleus decays by the emission of nucleons and fragments. As a result, free nucleons, LMF's, MMF's, and IMF's display a constant rise in their multiplicity. The HMF's are unstable and decay at a later time. It is also evident that lighter colliding nuclei saturate much faster than heavy nuclei. In addition, since balance energy in heavier nuclei is much smaller than that in lighter nuclei ($E_{\rm bal} \propto A^{-1/3}$), it takes longer time for heavier nuclei to saturate. One also notices that different fragments (except HMF's) are quite stable at such low incident energies; this is in contrast to high incident energies where IMF's and MMF's saturate only after 800 fm/c. The phase space is restricted in the domain of Fermi energy, and once frequent nucleon-nucleon collisions starts, matter breaks into pieces. As noted in Ref. [23], the average and maximal densities scale as $A^{-0.05182}$ and $A^{-0.11477}$ respectively, indicating that the compression reached at the balance energy is almost mass independent. However, the reaction time zone for $\rho/\rho_0 > 1$ varies as $A^{0.34}$, it is around 12 fm/c for ^{12}C+^{12}C, whereas it is 30 fm/c for

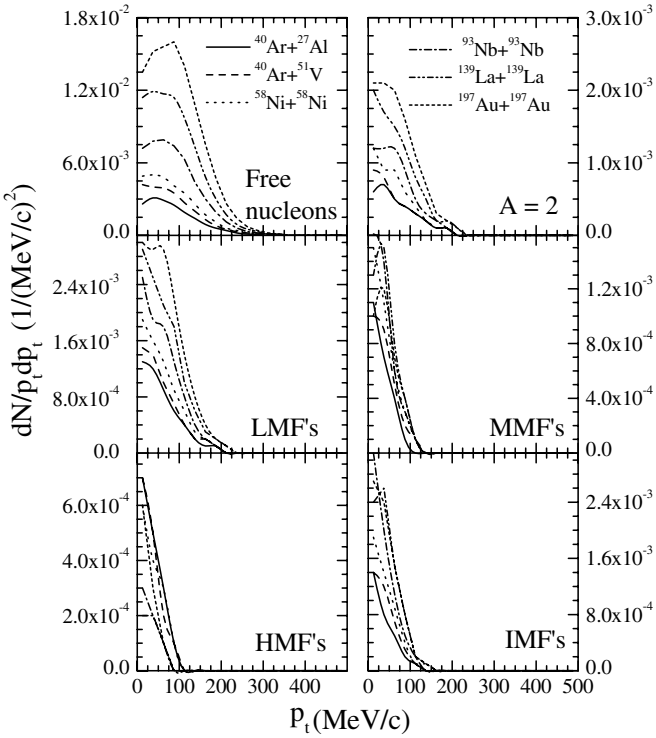

FIG. 3. $\frac{dN}{p_t dp_t}[1/(\mathrm{MeV}/c)^2]$ as a function of transverse energy p_t for the free nucleons, $A = 2$, LMF's, MMF's, HMF's, and IMF's for the reactions listed in Fig. 2.

^{197}Au+^{197}Au. This is not surprising since incident energy as well as initial velocity vary with same power factors. In other words, the cracks in the compound nucleus appear after the phase of high density. We have also examined the binding energy of all the fragments listed in Fig. 2. Independent of the masses of colliding nuclei, all fragments are reasonably bound. The average binding energy/nucleon is around -3 MeV/nucleon for LMF's, whereas it increases to around -8 MeV/nucleon for IMF's.

It would be of further interest to see the energy distribution of various fragments emitted at the balance energy. Figure 3 shows $\frac{dN}{p_t dp_t}$ vs p_t, where p_t is the mean transverse momentum. Here, we display the free nucleons, $A = 2$, LMF's, MMF's, HMF's, and IMF's. We see that, independent of the masses of colliding nuclei, the emitted nucleons and lighter fragments are more energetic than the heavier fragments. Furthermore, all the colliding nuclei emit fragments with similar endpoint tail energies pointing toward the uniformity in the velocity of fragments emitted at the balance energy. In addition, the shape is quite the same in all cases, which further strengthens homogeneity of the reaction dynamics at the balance energy.

In Fig. 4, we display the spectrum of rescaled longitudinal momentum in terms of rapidity distribution of fragments, where rapidity is defined as

$$Y(i) = \frac{1}{2} \ln \frac{\mathbf{E}(i) + \mathbf{p}_z(i)}{\mathbf{E}(i) - \mathbf{p}_z(i)}, \tag{14}$$

and $\mathbf{E}(i)$ and $\mathbf{p}_z(i)$ are, respectively, the total energy and longitudinal momentum of the i-th particle. We shall rather use a reduced rapidity $Y_{\rm red}(i) = Y(i)/Y_{\rm beam}$. We see, in part

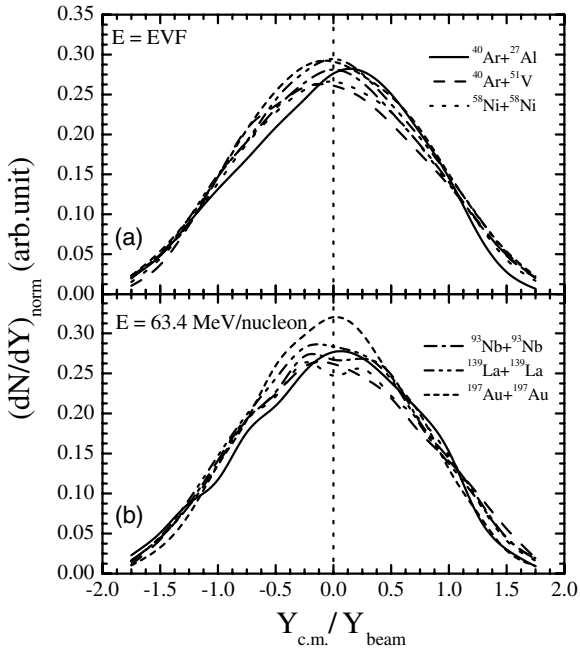

FIG. 4. Normalized rapidity distribution $\frac{1}{A_P+A_T}\frac{dN}{dY}$ as a function of $Y_{red}(i) = Y(i)/Y_{beam}$. Note that Y_{beam} depends upon the incident energy, which is different for every reaction. (a) Incident energy corresponds to theoretical balance energy. (b) Incident energy is fixed at 63.4 MeV/nucleon corresponding to the mean energy taken as the average of all theoretical balance energies.

(a) of the figure, that the rapidities of nucleons emitted in the reactions of ^{40}Ar+^{27}Al, ^{40}Ar+^{51}V, ^{58}Ni+^{58}Ni, ^{93}Nb+^{93}Nb, ^{139}La+^{139}La, and ^{197}Au+^{197}Au are quite similar, which again indicates similar dynamics at the balance point. If we perform a similar analysis at the average balance energy (taken as the average of different balance energies), we see in part (b) differences at the midrapidity region from where most of the fragments are emitted. It is worth mentioning that the nucleon-nucleon collisions causing the midrapidity emission follow a power law A^{τ} with τ close to unity.

Before coming to the energy of vanishing flow (EVF), let us examine the change in the multiplicity of different fragments with incident energy. We display, in Fig. 5, the emission of the largest fragments A^{max}, free nucleons, LMF's, and IMF's at the final stage of the reaction. We see well-accepted trends; with the increase in the incident energy, A^{max} starts downsizing; at over 120 MeV/nucleon (in the case of ^{40}Ar+^{45}Sc), it reduces to half its value. As a result, LMF emissions increase. This is also understandable since light mass fragments are created in the midrapidity region following the nucleon-nucleon collisions. However, the IMF emission either is due to the spectator matter or serves as a counterbalancing of the attractive and repulsive forces; therefore, after reaching a boiling off point in the ^{40}Ar+^{45}Sc reaction (typical IMF's are the remnant of projectile and target), it again drops down. This behavior is very prominent at higher incident energies where a clear rise and fall in the multiplicities of IMF's is observed with an increase in the incident energy as well as impact parameter. However, we do not see any typical structural changes at the energy of vanishing flow (marked by arrows in the figure). From the figure and also

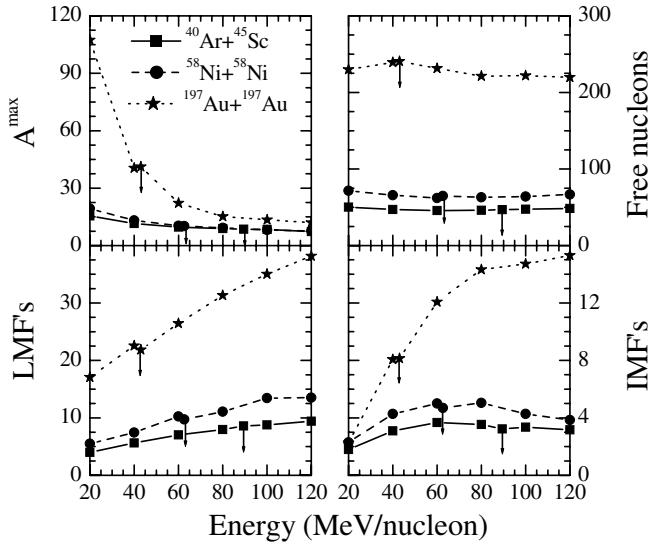

FIG. 5. Mean multiplicities of free nucleons, LMF's, and IMF's, and masses of the largest surviving fragments in simulations of ^{40}Ar+^{45}Sc, ^{58}Ni+^{58}Ni, and ^{197}Au+^{197}Au as a function of incident energy. Arrows show the balance energy in each case.

from other studies [25,35,37], it is clear that the variation of incident energy has a uniform and linear effect on the emission of fragments. As noted earlier, at low incident energies, the attractive mean field dominates; whereas at higher incident energies, repulsive nucleon-nucleon scattering dominates. The formation of complex fragments also results because of their mutual competition. If the attractive mean field dominates, it will produce very heavy fragments, whereas dominance of repulsive scatterings will shatter the matter into small pieces. At the balance energy, both these forces are counterbalanced; however, it is not reflected sharply in the emission of complex fragments.

Let us now understand the relation of multiplicities of different fragments with the mass of the colliding nuclei. For this study, we analyzed all the above cited reactions ranging between mass 63 and mass 394 at their corresponding theoretical balance energies and also at an average balance energy of 63.4 MeV/nucleon (calculated by averaging over all balance energies).

In Fig. 6, we display the free nucleons, $A = 2$, LMF's, MMF's, HMF's, and IMF's as a function of the system mass at their corresponding balance energies as well as at the fixed incident energy of 63.4 MeV/nucleon. All quantities except HMF's show increasing trends. In this low incident energy range (43–90 MeV/nucleon), all quantities (except HMF's) increase monotonically. If we merge both HMF's and IMF's, the new quantity will also increase monotonically with the size of the system. At very low incident energies, the Pauli principle hinders the opening of the phase space. As incident energy increases, the phase space opens up for binary nucleon-nucleon collisions, allowing the cracks to form, and then fragments of different sizes are produced. The point to note is that free nucleons as well as $A = 2$ show no energy dependence over the entire mass range. Whereas LMF's, MMF's, HMF's and IMF's do not show energy dependence for lighter colliding nuclei,

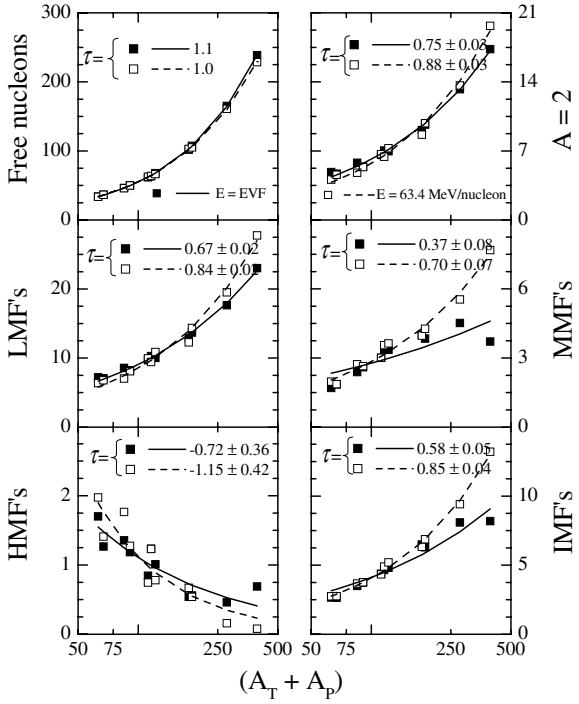

FIG. 6. Multiplicities of free nucleons, $A = 2$, LMF's ($2 \leqslant A \leqslant 4$), MMF's ($5 \leqslant A \leqslant 11$), HMF's ($15\% \leqslant A \leqslant 30\%$), and IMF's ($4 \leqslant A \leqslant 30\%$) as a function of composite mass of the colliding nuclei ($A_T + A_P$) for the reactions ^{36}Ar+^{27}Al, ^{40}Ar+^{27}Al, ^{40}Ar+^{45}Sc, ^{40}Ar+^{51}V, ^{64}Zn+^{48}Ti, ^{58}Ni+^{58}Ni, ^{64}Zn+^{58}Ni, ^{86}Kr+^{93}Nb,^{93}Nb+^{93}Nb, ^{139}La+^{139}La, and ^{197}Au+^{197}Au at the energy of vanishing flow (solid squares) and at a fixed energy 63.4 MeV/nucleon (open squares). The power law fits ($\propto A^{\tau}$) are also displayed in both cases as solid and dashed lines, respectively.

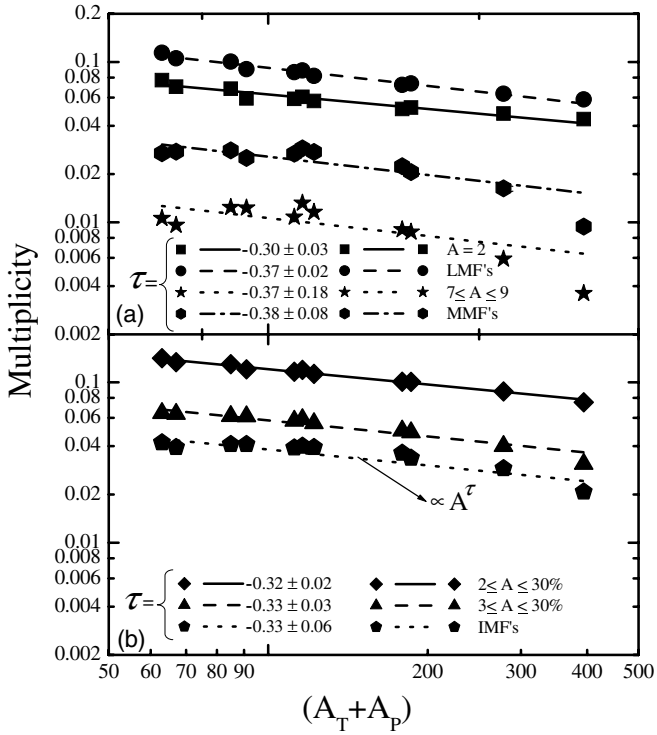

FIG. 7. Normalized multiplicities of $A = 2$, LMF's ($2 \leqslant A \leqslant 4$), ($7 \leqslant A \leqslant 9$), MMF's ($5 \leqslant A \leqslant 11$), ($2 \leqslant A \leqslant 30\%$), ($3 \leqslant A \leqslant 30\%$), and IMF's ($4 \leqslant A \leqslant 30\%$) as a function of composite size of the system ($A_T + A_P$) for all the reactions listed in Fig. 6. The power law fits are also conducted and displayed by lines in each case.

they have a strong energy dependence for heavier colliding nuclei. The energy-independent (or weakly dependent) nature points toward fewer nucleonic hard collisions (and available free phase space). One also notices that the multiplicities of LMF's, MMF's and IMF's are greater at 63.4 MeV/nucleon than at the balance energy for system masses $\geqslant$110 units, whereas HMF's show a reverse trend. The balance energy for masses $\geqslant$110 is around 40–60 MeV/nucleon, which is smaller than 63.4 MeV/nucleon. With an increase in the incident energy, more and more nucleon-nucleon binary collisions happen, leading to more medium mass fragments. It seems that the energy of 63.4 MeV/nucleon is too large for the emission of HMF's. These results agree with other theoretical and experimental findings [25,35,37]. As reported in Ref. [37], the mass dependence at a fixed incident energy yields a power law $\propto A^{\tau}$. We also obtain a similar dependence for the present case. Interestingly, even at the balance energy, a similar power law behavior can be seen with the power factor τ being less sensitive to the mass dependence. This is a remarkable observation. The present energy range (at balance point) varies from 89.4 MeV/nucleon for ^{40}Ar+^{45}Sc to 43 MeV/nucleon for ^{197}Au+^{197}Au. In spite of the difference of 46 MeV/nucleon, the power law dependence still holds.

In Fig. 7, we display the rescaled multiplicities of $A = 2$, LMF's, $7 \leqslant A \leqslant 9$, MMF's, along with masses $2 \leqslant A \leqslant 30\%$ and $3 \leqslant A \leqslant 30\%$ as well as IMF's. Interestingly, in all cases, a power law close to $(-1/3)$ is obtained. The deviation for heavier system masses points toward the exceeding role of Coulomb interactions in heavier colliding nuclei. It has been shown and discussed extensively in the literature that the mass yield curve approximately obeys a power law behavior $\propto A_{\mathrm{frag}}^{-\tau}$, i.e., the mass of different fragments [38]. It has been conjectured (though controversially) that this behavior (which has also been called "accidental" [38]) is an indication of the phase transition between gaseous and liquid phases of the nuclear matter. The power law dependence that we are discussing is something very different. The above power law function is for the multiplicity of a "given fragment" which scales with the size of the system. One should note that this power law ($\propto -1/3$) for the emission of different fragments at the energy of vanishing flow depicts the same mass-dependence trends as the energy of vanishing flow, for which the power factor is also close to $(-1/3)$. This factor emerges from the mutual dominance of the surface of the mean field $\propto (A^{2/3})$ and nucleon-nucleon scatterings $\propto A$, thus giving us a unique dependence $\propto (A^{-1/3})$ in all cases.

IV. SUMMARY

We presented the first-ever study of the emission of fragments at the energy of vanishing flow, i.e., a point in the energy scale where the attractive mean field (dominating at

the lower end of the energy scale) and repulsive nucleon-nucleon collisions (dominating at higher incident energies) counterbalance each other. This study was performed within the framework of the QMD model, which is reported to work well at low incident energies. Our findings clearly point toward a power law dependence of different fragment multiplicities at the energy of vanishing flow. This power factor τ ($\propto A^{\tau}$) is close to $(-1/3)$ suggesting again the mutual roles of the mean field and collisions in the formation of fragments at the balance point. This dependence is similar to the one reported for the mass dependence of the energy of vanishing flow.

ACKNOWLEDGMENT

Work supported by CSIR, Govt. of India under grant no: 7167/NS-EMR-II/2006.

[1] J. J. Molitoris and H. Stöcker, Phys. Lett. **B162**, 47 (1985); G. F. Bertsch, W. G. Lynch, and M. B. Tsang, Phys. Lett. **B189**, 384 (1987).
[2] C. A. Ogilvie *et al*., Phys. Rev. C **42**, R10 (1990).
[3] G. D. Westfall *et al*., Phys. Rev. Lett. **71**, 1986 (1993).
[4] J. C. Angelique *et al*., Nucl. Phys. **A614**, 261 (1997).
[5] A. Buta *et al*., Nucl. Phys. **A584**, 397 (1995).
[6] J. P. Sullivan *et al*., Phys. Lett. **B249**, 8 (1990).
[7] D. J. Magestro, W. Bauer, and G. D. Westfall, Phys. Rev. C **62**, 041603(R) (2000).
[8] R. Pak *et al*., Phys. Rev. Lett. **78**, 1022 (1997); R. Pak, O. Bjarki, S. A. Hannuschke, R. A. Lacey, J. Lauret, W. J. Llope, A. Nadasen, N. T. B. Stone, A. M. Vander Molen, and G. D. Westfall, Phys. Rev. C **54**, 2457 (1996); R. Pak *et al*., *ibid.* **53**, R1469 (1996).
[9] D. Krofcheck *et al*., Phys. Rev. C **43**, 350 (1991).
[10] Z. Y. He *et al*., Nucl. Phys. **A598**, 248 (1996).
[11] D. Cussol *et al*., Phys. Rev. C **65**, 044604 (2002).
[12] D. Krofcheck *et al*., Phys. Rev. C **46**, 1416 (1992).
[13] D. J. Magestro, W. Bauer, O. Bjarki, J. D. Crispin, M. L. Miller, M. B. Tonjes, A. M. Vander Molen, G. D. Westfall, R. Pak, and E. Norbeck, Phys. Rev. C **61**, 021602(R) (2000).
[14] W. M. Zhang *et al*., Phys. Rev. C **42**, R491 (1990); M. D. Partlan *et al*., Phys. Rev. Lett. **75**, 2100 (1995); P. Crochet *et al*., Nucl. Phys. **A624**, 755 (1997).
[15] B. A. Li, Phys. Rev. C **48**, 2415 (1993).
[16] V. de la Mota, F. Sebille, M. Farine, B. Remaud, and P. Schuck, Phys. Rev. C **46**, 677 (1992).
[17] H. M. Xu, Phys. Rev. C **46**, R389 (1992); H. M. Xu, Phys. Rev. Lett. **67**, 2769 (1991).
[18] H. Zhou, Z. Li, Y. Zhuo, and G. Mao, Nucl. Phys. **A580**, 627 (1994).
[19] E. Lehmann, A. Faessler, J. Zipprich, R. K. Puri, and S. W. Huang, Z. Phys. A **355**, 55 (1996).
[20] S. Soff, S. A. Bass, C. Hartnack, H. Stöcker, and W. Greiner, Phys. Rev. C **51**, 3320 (1995); A. D. Sood and R. K. Puri, Eur. Phys. J. A (in press).
[21] S. Kumar, M. K. Sharma, R. K. Puri, K. P. Singh, and I. M. Govil, Phys. Rev. C **58**, 3494 (1998).
[22] A. D. Sood and R. K. Puri, Phys. Lett. **B594**, 260 (2004); A. D. Sood and R. K. Puri, Phys. Rev. C **69**, 054612 (2004).
[23] A. D. Sood and R. K. Puri, Phys. Rev. C **70**, 034611 (2004); Int. J. Mod. Phys. E (in press).
[24] A. Bonasera and L. P. Csernai, Phys. Rev. Lett. **59**, 630 (1987); Nucl. Phys. **A478**, 159 (1988); M. Belkacem, V. Latora, and A. Bonasera, in *Advances in Nuclear Dynamics 1, Proceedings of the XI Winter Meeting in Nuclear Dynamics, 1995*, edited by B. Arruada and A. Mignerey (Springer, New York, 1996).
[25] P. B. Gossiaux and J. Aichelin, Phys. Rev. C **56**, 2109 (1997).
[26] J. Aichelin, Phys. Rep. **202**, 233 (1991); C. Hartnack, R. K. Puri, J. Aichelin, J. Konopka, S. A. Bass, H. Stöcker, and W. Greiner, Eur. Phys. J. A **1**, 151 (1998).
[27] R. K. Puri and S. Kumar, Phys. Rev. C **57**, 2744 (1998); Zhuxia Li, C. Hartnack, H. Stöcker, and W. Greiner, *ibid.* **44**, 824 (1991).
[28] C. Liewen, Z. Fengshou, and J. Genming, Phys. Rev. C **58**, 2283 (1998).
[29] S. Kumar, R. K. Puri, and J. Aichelin, Phys. Rev. C **58**, 1618 (1998).
[30] T. Maruyama, A. Bonasera, M. Papa, and S. Chiba, Eur. Phys. J. A **14**, 191 (2002).
[31] B. A. Li and A. T. Sustich, Phys. Rev. Lett. **82**, 5004 (1999); Y. M. Zheng, C. M. Ko, B. A. Li, and B. Zhang, Phys. Rev. Lett. **83**, 2534 (1999).
[32] H. Zhou, Z. Li, and Y. Zhuo, Phys. Rev. C **50**, R2664 (1994).
[33] H. W. Barz, J. P. Bondorf, D. Idier, and I. N. Mishustin, Phys. Lett. **B382**, 343 (1996).
[34] C. Roy *et al*., Z. Phys. A **358**, 73 (1997).
[35] J. Singh, S. Kumar, and R. K. Puri, Phys. Rev. C **62**, 044617 (2000); J. Singh and R. K. Puri, *ibid.* **62**, 054602 (2000); S. Kumar and R. K. Puri, *ibid.* **58**, 320 (1998).
[36] R. K. Puri, C. Hartnack, and J. Aichelin, Phys. Rev. C **54**, R28 (1996); P. B. Gossiaux, R. K. Puri, Ch. Hartnack, and J. Aichelin, Nucl. Phys. **A619**, 379 (1997); R. K. Puri and J. Aichelin, J. Comput. Phys. **162**, 245 (2000).
[37] J. Singh and R. K. Puri, Phys. Rev. C **65**, 024602 (2000); J. Singh, R. K. Puri, and J. Aichelin, Phys. Lett. **B519**, 46 (2001).
[38] A. Bohnet, J. Aichelin, J. Pochodzalla, W. Trautmann, G. Peilert, H. Stocker, and W. Greiner, Phys. Rev. C **44**, 2111 (1991); G. Peilert, H. Stocker, W. Greiner, A. Rosenhauer, A. Bohnet, and J. Aichelin, *ibid.* **39**, 1402 (1989).